PAGEOPH, Vol. 138, No. 4 (1992) 0033–4553/92/040679–28$1.50 + 0.20/0

Fractures: Finite-size Scaling and Multifractals

L. J. PYRAK-NOLTE,[1] L. R. MYER,[2] and D. D. NOLTE[3]

Abstract—The distributions of contact area and void space in single fractures in granite rock have been determined experimentally by making metal casts of the void spaces between the fracture surfaces under normal loads. The resulting metal casts on 52 cm diameter core samples show a complex geometry for the flow paths through the fracture. This geometry is analyzed using finite-size scaling. The spanning probabilities and percolation probabilities of the metal casts are calculted as functions of observation scale. Under the highest stresses of 33 MPa and 85 MPa there is a significant size-dependence of the geometric flow properties for observation scales smaller than 2 mm. Based on this data, the macroscopic percolation properties of the extended fracture can be well represented by relatively small core samples, even under normal stresses larger than 33 MPa. The metal casts also have rich multifractal structure that changes with changing stress.

Key words: Fractures, fractals, multifractals, scaling, percolation, geohydrology, rock mechanics, permeability.

1. Introduction

A major practical obstacle in studying fluid flow through geologic formations is the problem of relating laboratory measurements to behavior observed in the field. Laboratory measurements are performed on relatively small specimens with sizes from millimeters to many centimeters. Fluid flow through geologic formations, on the other hand, may occur over tens to thousands of meters. Do the laboratory measurements relate to the macroscopic behavior observed in the field, or do different mechanisms dominate on different scales? Can hydraulic measurements performed in the laboratory on core samples be used to qualitatively predict behavior *in situ*?

These are questions of scale effects and size dependence of fluid flow through fractures. Fractures in geologic formations are often the main conduits along which fluids move through a rock mass. Relatively few investigators have examined the effect of the scale of observation on fluid flow through fractures. Experimental evidence (WITHERSPOON *et al.*, 1979; RAVEN and GALE, 1985) shows opposing

[1] Department of Civil Engineering and Geological Sciences, University of Notre Dame, Notre Dame, IN 46556.
[2] Earth Science Division, Lawrence Berkeley Laboratory, Berkeley, CA 94720, U.S.A.
[3] Department of Physics, Purdue University, West Lafayette, IN 47907-1396, U.S.A.

trends with hydraulic conductivity increasing or decreasing with increasing sample size. From a numerical investigation, NEUZIL and TRACEY (1981) concluded that smaller specimens will have smaller values of conductivity than larger specimens under the same stress because fewer large flow channels exist. From a theoretical study of the effect of sample size on the hydraulic and deformation properties of a single fracture, TSANG and WITHERSPOON (1983) determined that large-scale roughness of the fracture controls the hydraulic and mechanical properties of the fracture. They concluded that if the rock specimen is smaller than the characteristic roughness scale then the fluid flow measurements made on the specimen will not be representative of the large fracture behavior.

The study of scale effects is an integral part of percolation theory and in particular the study of finite-size scaling in percolation systems (STAUFFER, 1985). The flow paths in a fracture represent a complex geometric structure with local connections and long-range conductivity or permeability. The geometric properties of the flow paths (including the size dependence) are closely related to the hydraulic properties. The problem of analyzing such complicated geometric structures is a standard component of percolation theory. Percolation systems show critical behavior. Below a critical density (the percolation threshold) the pattern is not connected and no flow occurs. Critical systems are well-known to obey scaling laws, especially when the system is close to the critical threshold (STANLEY, 1971). In particular, the probability that a connected path exists across the pattern is a function of the sample size. The size dependence of this spanning probability can be used to identify the scaling behavior of the hydraulic properties of the system as the sample size is increased from laboratory scales to field scales.

The void space geometry in a fracture is not immediately identifiable with standard percolation models. The void spaces in a fracture are strongly heterogeneous and correlated. The void geometry of a fracture will be influenced by the roughness of the individual surfaces and by the correlations between the surfaces (SWAN, 1983; BROWN *et al.*, 1986). A natural choice for studying the scale effects on fluid flow through fractures is to use fractal analysis to study the size effects on fracture void geometry. BROWN and SCHOLZ (1985) measured surface roughness of several fractures and determined that surface roughness was scale independent and fractal within a certain range of sizes. Fracture geometries may not be describable in terms of a single fractal dimension. Different subsets of the fracture geometry may have different fractal dimensions. This property is called multiscaling, in which different components of the structure scale differently with size. Such structures are called multifractal. Multifractals often arise under conditions of random multiplicative processes (REDNER, 1990), such as cascades, or successive sequences of rupture or erosion. Therefore the multifractal properties of fracture geometries may be related to the processes and conditions under which the fracture formed.

In this paper, we discuss the importance of considering the size-dependence of geometrical properties (such as the spanning probability) for the void spaces within a fracture. The experimental apparatus for obtaining metal casts of the fracture is described in Section 2. In Section 3 we use finite-size scaling theory to determine the percolation properties of the experimental data to study the scale effects on percolation through fractures. This analysis yields results on the scale effects of fluid flow through fractures. We perform multifractal analysis of the contact areas in the single natural fractures in Section 4.

2. Experimental Data

A metal injection technique was used to determine contact area of two natural fractures (denoted as E30 and E32) in quartz monzonite (Stripa granite), as a function of stress. The specimens measured 52 mm in diameter by 77 mm in height and each contained a single natural fracture orthogonal to the long axis of the core. Measurements of void space geometry were made for effective stresses of 3 MPa, 33 MPa, and 85 MPa. The metal used to fill the fracture void spaces is one of a family of bismuth-lead-tin alloys of which Wood's metal is the most commonly recognized. In the liquid phase these metals are nonwetting with an effective surface tension of 0.282 N/m (YADAV *et al.*, 1984). The nominal composition of the particular metal used was 0.42 Bi, 0.38 Pb, 0.11 Sn, and 0.08 Cd. The alloy [Cerrosafe®] used in these experiments has a melting point of 160° to 190°F, a Young's modulus of 9.7 GPa, and a density of 9.4 g/cm^3. This Wood's metal injection technique is similar to mercury porosimetry methods, but has the advantage of yielding metal casts of the void space for the same fracture under different stress. These casts can then be studied in detail. Wood's metal injection techniques have been used by other investigators (DULLIEN, 1981; SWANSON, 1979; YADAV et al.; 1984; PYRAK-NOLTE *et al*, 1987; ZHENG, 1989; PYRAK-NOLTE, 1991) to study pores, cracks and fractures in rock.

Figure 1 is a diagram of the experimental set-up. The specimen is held in a triaxial test vessel in the frame of a test machine and an axial load is applied normal to the fracture surface. The vessel is maintained at a temperature just above the melting point of the alloy. To perform an injection test, the vessel is evacuated and molten metal is pumped into the test vessel until the desired pore pressure is obtained. The uniaxial load and the pore pressure are maintained while the metal is allowed to solidify. When the specimen is removed from the vessel, the two halves of the specimen are separated to examine the metal casts of the void spaces corresponding to the effective stress of the test.

The distribution of the metal on the two fracture surfaces was examined using a scanning electron microscope (SEM). Because some casts of the void spaces adhere to one surface and some to the other, composite SEM micrographs were made to determine contact area and void space distribution. The composite micrographs were formed by superimposing images of each surface for the same

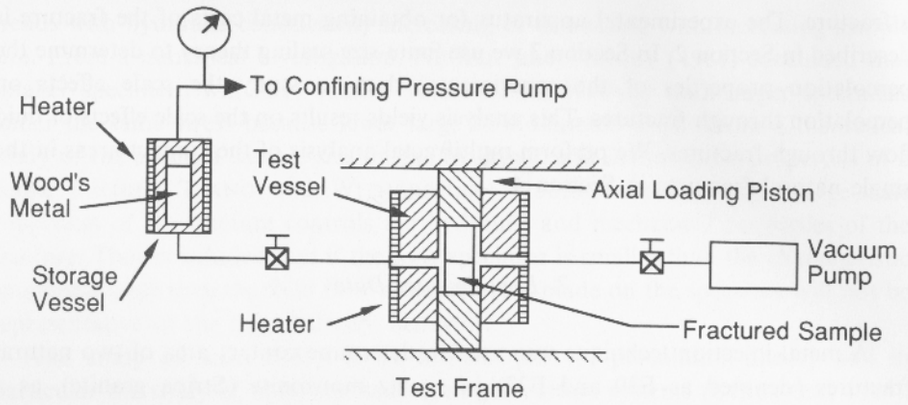

Figure 1
Experimental apparatus to obtain the contact areas in the fractured core samples.

location. Figure 2 contains micrographs for specimens E30 showing the distributed contact area for effective stresses of 3 MPa, 33 MPa, and 85 MPa. The results for specimen E32 are shown in Figure 3. The white regions represent contact area while the black regions represent where the metal penetrated.

In order to perform the percolation and multifractal analysis of the experimental data, the SEM micrographs were digitized using a Macintosh Applescanner. The micrographs were scanned at a resolution of 200 dots/inch using Appelscan software version 1.02. The files were saved as tagged information formatted files (TIFF). The TIFF files were exported into PostScript format, the line breaks were removed from the files and the files were saved as text. The data files were read using a program written in PASCAL. Output from this consisted of a 300×300 binary array representing the black and white portions of the micrographs. The analysis was performed for several different regions of each micrograph.

3. *Finite-size Scaling*

A fundamental aspect of percolating systems is the dependence of the percolation properties on the size of the system. Percolation theory is a formalism which treats the probability that a random system can support flow from one side to the other. Percolation probabilities are defined as functions of the pattern occupancy, p. The occupancy, p, is the fraction of the pattern that can be occupied by a fluid, for example the void spaces between the surfaces of a fracture. A central feature of percolation theory is the critical threshold, p_c. When the occupancy is smaller than p_c (that is, $p - p_c < 0$) then connected paths across the pattern are unlikely to occur. For occupancies $p - p_c > 0$ a connected path is likely to exist, and the

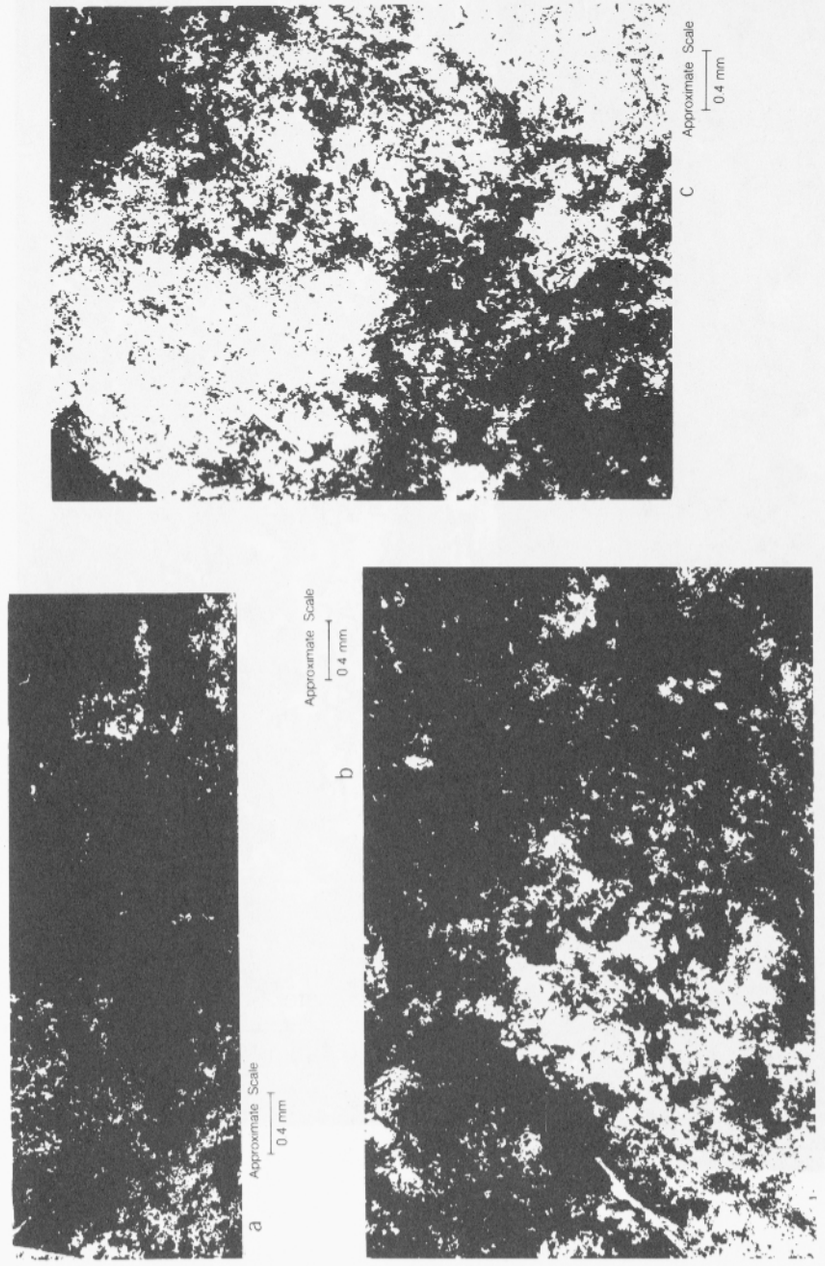

Figure 2
Experimental micrographs of the contact areas in two fractures in quartz monzonite granite from Stripa, Sweden for varying stresses. Specimen E30 was subjected to different stresses corresponding to (a) E30 at 3 MPa, (b) E30 at 33 MPa, and (c) E30 at 85 MPa. Regions of white represent contact area and black regions represent void spaces.

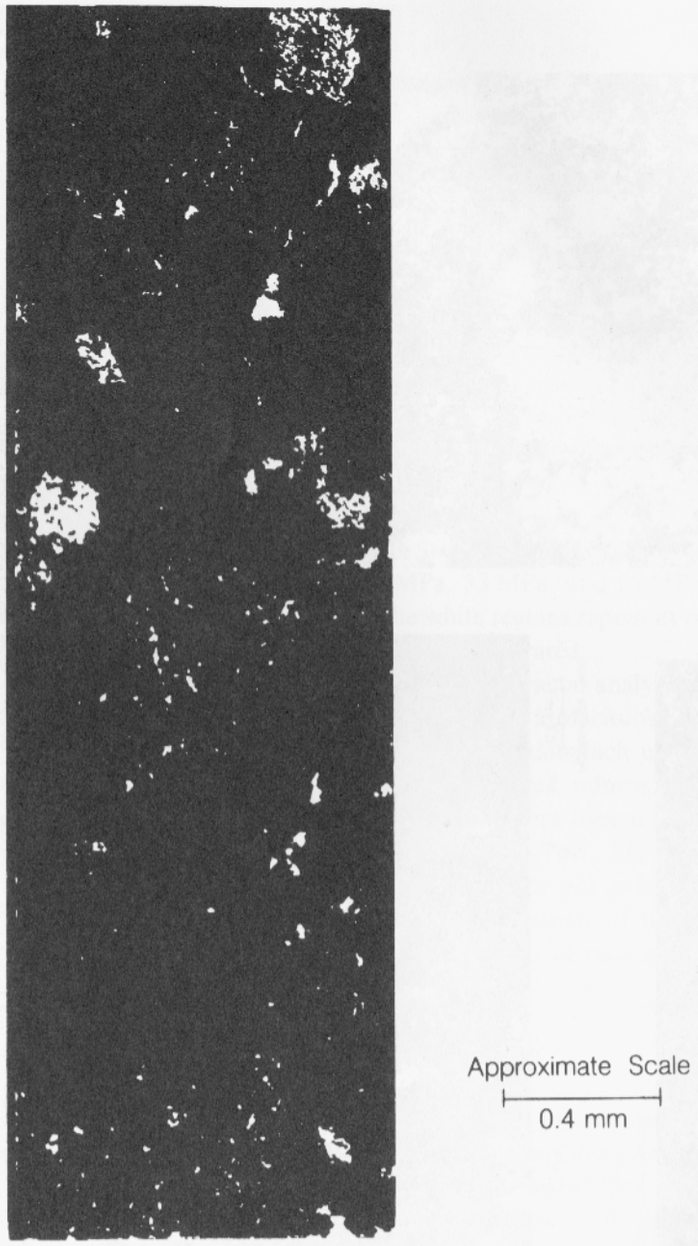

Figure 3(a)

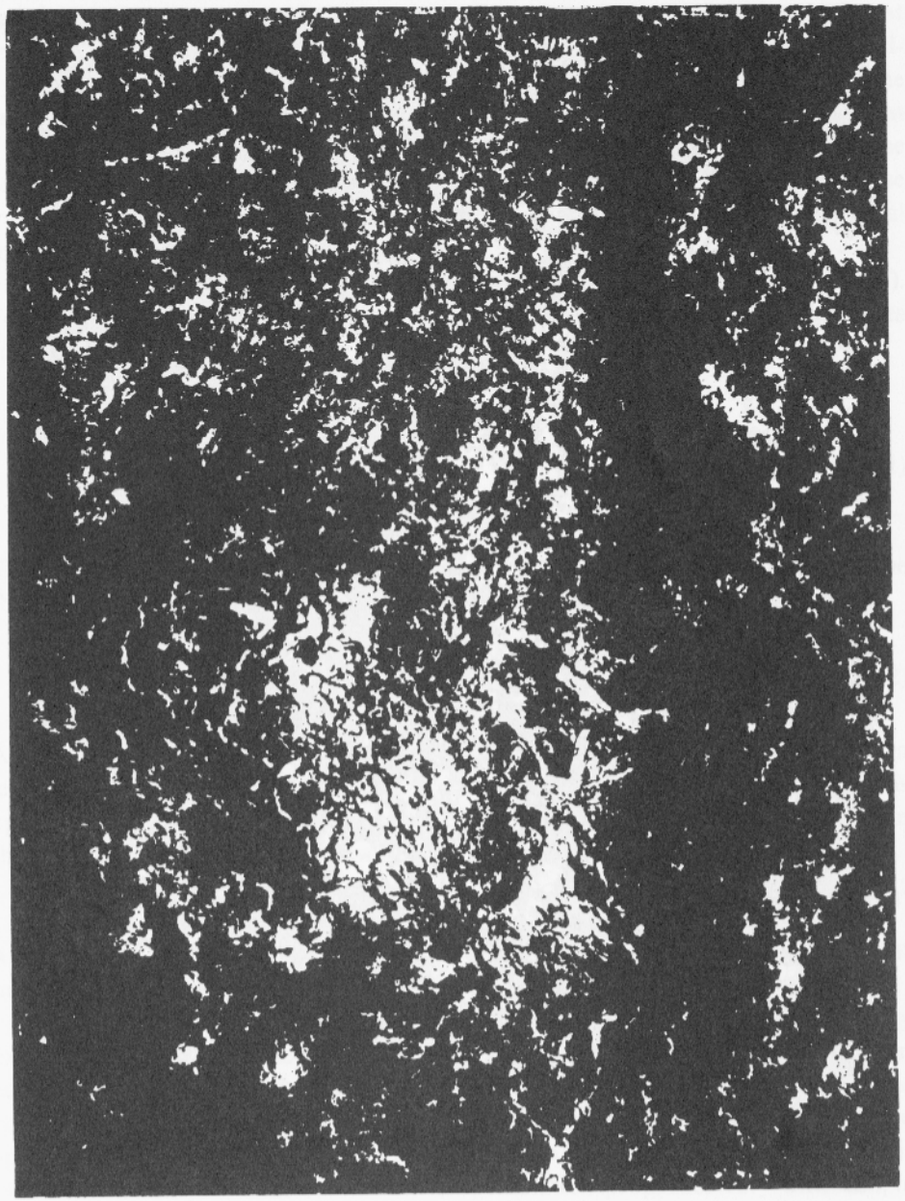

Figure 3(b)

Figure 3(c)

Figure 3
Specimen E32 was subjected to different stresses corresponding to (a) E32 at 3 MPa, (b) E32 at 33 MPa and (c) E32 at 85 MPa.

pattern is said to percolate. It is convenient for this article to define three different percolation probabilities: R, P, and Σ. The probability R is the spanning probability. This is the probability that a connected path exists across the fracture. The probability P is the strength of the percolating cluster. This is the probability that a site chosen at random belongs to the percolating cluster. The strength of the percolating cluster is analogous to the order parameter in thermodynamic phase transitions (STAUFFER, 1985). Finally, the conductivity Σ is related to the electrical conductivity of the pattern.

These three percolation probabilities R, P, and Σ vary as functions of $(p - p_c)$. For systems that are infinitely large, i.e., the system size $L \to \infty$, these probabilities vary as

$$R = \begin{cases} 0 & (p - p_c) < 0 \\ 1 & (p - p_c) > 0 \end{cases}$$
$$P \propto (p - p_c)^{\beta} \tag{1}$$
$$\Sigma \propto (p - p_c)^{\mu}.$$

The exponents β and μ are called critical exponents. In two dimensions it can be shown that (see STAUFFER, 1985) they have the values

$$\beta = 5/36 = 0.14$$
$$\mu = 1.3. \tag{2}$$

Another important parameter in randomly connected systems is the correlation length ξ. For our rock specimens above threshold, the correlation length is approximately equal to the average size of the contact areas. Near the percolation threshold the correlation length varies as

$$\xi \propto (p - p_c)^{-\nu} \tag{3}$$

where $\nu = 4/3$ is the correlation length exponent. From equation (3) it is seen that in the limit as $p \to p_c$ the correlation length diverges.

In practice, it is not possible to work with infinitely large systems. Any experimental random pattern must be a sample of a finite-size. The expressions in equation (1) are only valid for systems whose linear size L is much greater than the correlation length $L \gg \xi$. If the correlation length becomes larger than the core specimen size, then effects of changing specimen size will be important and it becomes necessary to understand how the percolation properties vary with sample size. Specifically with respect to fluid flow through single fractures, one would like to be able to take a relatively small core sample of a fracture and predict what the macroscopic percolation properties of the fracture would be across meters or more.

Finite-size scaling is an intrinsic part of percolation theory because real percolation systems are finite. The concepts of finite-size scaling fall collectively under the title of renormalization (PFEUTY *et al.*, 1975; WILSON, 1975, 1979). Renormaliza-

Figure 3(c)

Figure 3
Specimen E32 was subjected to different stresses corresponding to (a) E32 at 3 MPa, (b) E32 at 33 MPa and (c) E32 at 85 MPa.

pattern is said to percolate. It is convenient for this article to define three different percolation probabilities: R, P, and Σ. The probability R is the spanning probability. This is the probability that a connected path exists across the fracture. The probability P is the strength of the percolating cluster. This is the probability that a site chosen at random belongs to the percolating cluster. The strength of the percolating cluster is analogous to the order parameter in thermodynamic phase transitions (STAUFFER, 1985). Finally, the conductivity Σ is related to the electrical conductivity of the pattern.

These three percolation probabilities R, P, and Σ vary as functions of $(p - p_c)$. For systems that are infinitely large, i.e., the system size $L \to \infty$, these probabilities vary as

$$R = \begin{cases} 0 & (p - p_c) < 0 \\ 1 & (p - p_c) > 0 \end{cases}$$

$$P \propto (p - p_c)^{\beta} \tag{1}$$

$$\Sigma \propto (p - p_c)^{\mu}.$$

The exponents β and μ are called critical exponents. In two dimensions it can be shown that (see STAUFFER, 1985) they have the values

$$\beta = 5/36 = 0.14$$
$$\mu = 1.3. \tag{2}$$

Another important parameter in randomly connected systems is the correlation length ξ. For our rock specimens above threshold, the correlation length is approximately equal to the average size of the contact areas. Near the percolation threshold the correlation length varies as

$$\xi \propto (p - p_c)^{-\nu} \tag{3}$$

where $\nu = 4/3$ is the correlation length exponent. From equation (3) it is seen that in the limit as $p \to p_c$ the correlation length diverges.

In practice, it is not possible to work with infinitely large systems. Any experimental random pattern must be a sample of a finite-size. The expressions in equation (1) are only valid for systems whose linear size L is much greater than the correlation length $L \gg \xi$. If the correlation length becomes larger than the core specimen size, then effects of changing specimen size will be important and it becomes necessary to understand how the percolation properties vary with sample size. Specifically with respect to fluid flow through single fractures, one would like to be able to take a relatively small core sample of a fracture and predict what the macroscopic percolation properties of the fracture would be across meters or more.

Finite-size scaling is an intrinsic part of percolation theory because real percolation systems are finite. The concepts of finite-size scaling fall collectively under the title of renormalization (PFEUTY *et al.*, 1975; WILSON, 1975, 1979). Renormaliza-

tion group theory was developed to study phase transitions and critical phenomena (WILSON, 1974). At the heart of renormalization is the scaling hypothesis. This states that a critical probability P that depends on the variables $(p - p_c, L)$ has the scaling form

$$P = L^{-A} F[(p - p_c) L^B] \tag{4}$$

close to the critical threshold. Equation (4) is a general scaling hypothesis. For specific systems, such as two-dimensional percolation systems, the exponents A and B differ for the different critical probabilities. The finite-size scaling ($L \leq \xi$) probabilities analogous to those of the infinite system are

$$\begin{aligned} R &= H[(p - p_c) L^{1/\nu}] \\ P &= L^{-\beta/\nu} G[(p - p_c) L^{1/\nu}] \\ \Sigma &= L^{-\mu/\nu} F[(p - p_c) L^{1/\nu}] \end{aligned} \tag{5}$$

where $H((p - p_c)L^{1/\nu})$, $G((p - p_c)L^{1/\nu})$ and $F((p - p_c)L^{1/\nu})$ are scaling functions that can be obtained from numerical computation.

The scaling functions in equation (5) remain finite when $(p - p_c) = 0$. Thus, at the threshold the relationship between sample size and the scaling probabilities becomes simply

$$\begin{aligned} R &= \text{const} \\ P &\propto L^{-\beta/\nu} \\ \Sigma &\propto L^{-\mu/\nu}. \end{aligned} \tag{6}$$

The constant value for the spanning probability R is called the renormalization fixed point. The spanning probability at the threshold is scale invariant. This also means that the pattern is scale invariant, or fractal, as $\xi \to \infty$. The cluster strength P and the conductivity Σ both decrease with increasing sample size.

The decrease of the percolation probability and conductivity with increasing size is a general property that applies as well when $p \neq p_c$. This is the case for systems both above and below threshold. For systems far above the threshold, the probability $P = 1$. In contrast, the spanning probability R increases with increasing L for $(p - p_c) > 0$ (above the threshold), but decreases with increasing L for $(p - p_c) < 0$ (below the threshold). These properties are illustrated in Figure 4 for Stratified Continuum percolation (NOLTE and PYRAK-NOLTE, 1991) which is an ideal correlated percolation system. The figure shows that the finite sample size smears out the sharp percolation threshold, allowing a finite percolation probability for $p \leq p_c$. Note that for $p \gg p_c$, the percolation probabilities do not vary appreciably with sample size. Though shown here only for purposes of illustration, the Stratified Continuum percolation model also shares many of the properties of the experimental system shown in Figures 2 and 3.

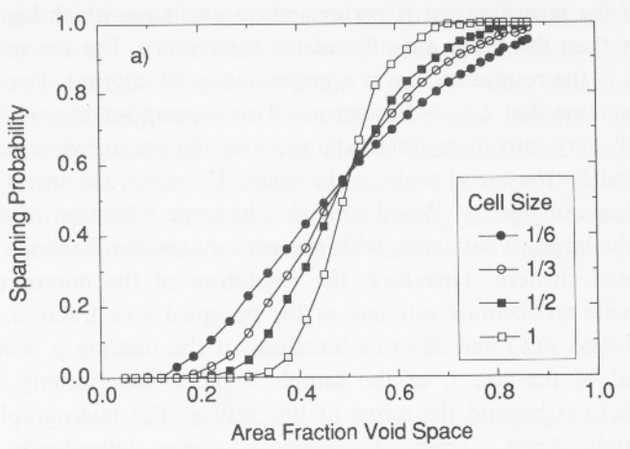

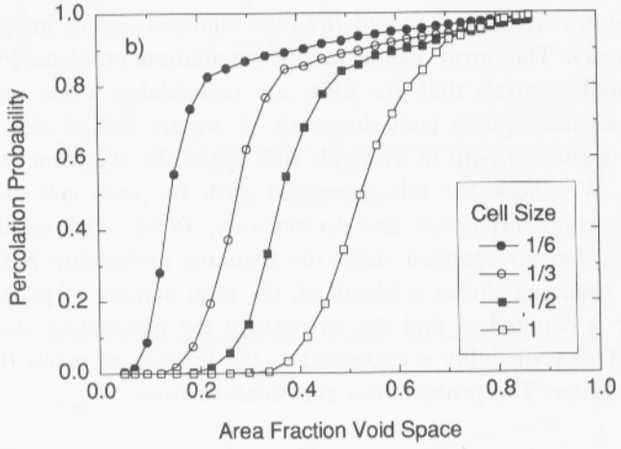

Figure 4
Spanning probability (a) and percolation probability (b) for the stratified percolation model with three tiers as functions of the area fraction. The fixed point in the spanning probability occurs at the threshold $A_c = 0.5$.

By analyzing the experimental micrographs of Figures 2 and 3 using the ideas of finite-size scaling, an understanding of the percolation properties of the macroscopic parent fractures can be gained. In addition, the proximity of the patterns to the threshold can be evaluated. This analysis requires the determination of the occupancy, p, in the figures which is equivalent to the fractional area A covered by void space. It is important to note that measuring area fractions of a two-dimensional fractal structure is not well-defined. An accurate value for the area can only

be obtained if the measurement is performed on an image which has a resolution that is smaller than the lower cut-off scale of the pattern. For the micrographs in Figures 2 and 3, the resolution size is approximately 10 microns. For our analysis, we therefore assume that $L_{\min} > 10$ microns. This assumption cannot be rigorously justified, which may introduce systematic error in the measured value of the area fraction covered by the metal casts of the voids. However, the metal casts consist of a finite volume of injected Wood's metal. The largest fraction of the volume is contained in the largest void areas, with successively smaller fractions contained in the smaller void clusters. Therefore, the resolution of the micrographs are expected to provide an accurate estimate of the occupied area fraction.

We have found $P(L)$ and $R(L)$ as functions of the fraction p occupied by the metal cast and of the size L of the sample regions. Determining the electrical conductivity $\Sigma(L)$ is beyond the scope of this article. The micrographs have sizes of approximately 4 mm × 2 mm. To evaluate a size dependence, successively smaller regions of the figures were examined. We chose square cell sizes L of approximately 2 mm, 1 mm, 0.67 mm, and 0.33 mm. The total fractional void area of Figures 2 and 3 ranges from a minimum of 62% to a maximum of 95%.

To find the probabilities $P(L)$ and $R(L)$ the digitized sample image is read into a 300 × 300 array. This array defines a site percolation problem. Pixels that are black are available; pixels that are white are unavailable. Flow can only occur between two adjacent pixels (not diagonal). A square cell of side L is said to percolate if a connected path of available sites spans the cell from one side to the opposite side. We check for this connected path for each cell using a cluster numbering algorithm (HOSHEN and KOPELMAN, 1976). The tabulation of the number of cells that are spanned yields the spanning probability $R(L)$ for the cell size. Once the spanning cluster is identified, the total number of pixels that belong to that cluster is counted to find the strength of the percolating cluster $P(L)$ for that cell size. This probability is expressed as the fraction of pixels that belong to the spanning cluster. The probabilities are obtained from

$$P(L) = \frac{\sum_{i=1}^{b^2} d_i(L)}{b^2} \tag{7}$$

$$R(L) = \frac{\sum_{i=1}^{b^2} g_i(L)}{b^2} \tag{8}$$

where the scale factor $b = 1, 2, 3, 6$. For our patterns, the observation lengths are approximately $L = 2$ mm, 1 mm, 0.67 mm, and 0.33 mm. The value of $d_i(L)$ is equal to the fraction of sites that belong to the spanning cluster of the ith cell of size L. The variable $g_i(L) = 1$ if the ith cell percolates, and $g_i(L) = 0$ if it does not.

The probabilities for the micrographs in Figures 2 and 3 are shown in Figures 5 and 6 as functions of cell size. The high-stress micrographs show variations as the cell size is changed from 0.67 mm to 2 mm. The low-stress micrographs, on the other hand, have relatively weak size dependence. For the spanning probability, the probabilities increase with increasing cell size. It becomes more likely that the cell will contain the infinite cluster as its size increases. The strength of the percolating cluster, on the other hand, decreases with increasing cell size. Some clusters that span a small cell do not belong to the infinite cluster, and these clusters will not be

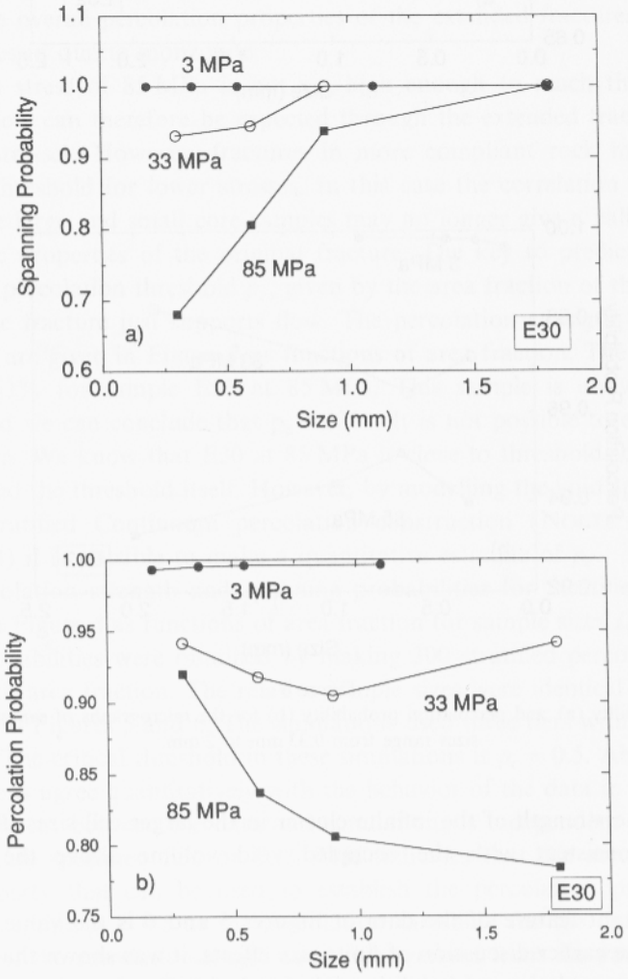

Figure 5
Spanning probability (a) and percolation probability (b) for the micrographs of sample E30 as functions of the size of the cell. The cell sizes range from 0.33 mm to 2 mm.

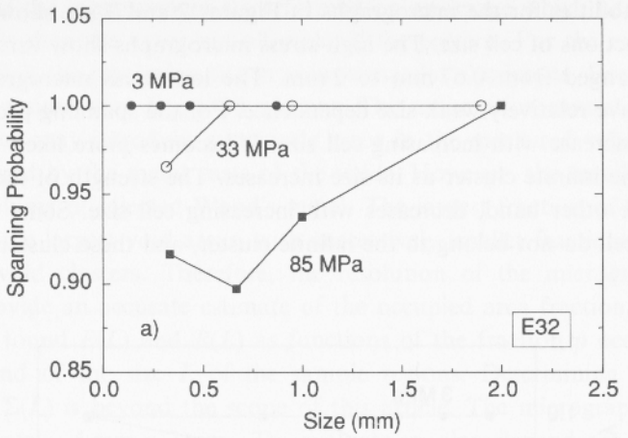

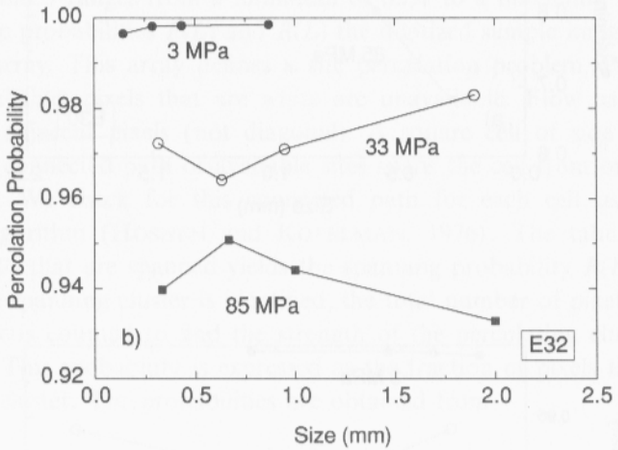

Figure 6
Spanning probability (a) and percolation probability (b) for the micrographs of sample E32. The cell sizes range from 0.33 mm to 2 mm.

included in the strength of the infinite cluster in the larger cell sizes. Both of these trends are consistent with the occupied void volume above the percolation threshold.

An important feature of the data in Figures 5 and 6 is the value at large cell sizes. From the earlier discussion of finite-size effects, it was shown that a finite size influences the percolation probabilities only for $L \lessapprox \xi$. For $L \gg \xi$, the probability is equal to the average over the cell. The percolation probability for sample E30 at high stress shows asymptotic behavior, indicating that the fracture is relatively close

to the percolation threshold. The data for the micrographs of sample E32, on the other hand, show no significant size dependence, implying that $L > \xi$. These conclusions from the percolation strength are corroborated by the spanning probability. For both E30 and E32, $R = 1$ for $L = 2$ mm, indicating that $\xi < 2$ mm in all cases. This result has significant implications for predicting flow properties of the macroscopic parent fractures. The size of the core samples is larger than ξ for all cases considered here. The two-dimensional conductivity Σ (related to the permeability) measured for the core sample should therefore be equal to the conductivity of the macroscopic fracture, with no further scale dependence. Because this holds even for the highest stress, this suggests that relatively small core samples are valid probes of the overall percolation properties of the extended fractures, at least for these fractures in quartz monzonite.

The high stress of 85 MPa is not yet high enough to reach the percolation threshold. Flow can therefore be expected through the extended fracture even for these large stresses. However, fractures in more compliant rock may reach the percolation threshold for lower stresses. In this case the correlation length ξ may become quite large and small core samples may no longer give a valid measure of the hydraulic properties of the original fracture. The key to predictions of scale effects is the percolation threshold p_c, given by the area fraction of the void spaces for which the fracture just supports flow. The percolation strength and spanning probabilities are given in Figure 7 as functions of area fraction. The smallest area fraction is 62% for sample E30 at 85 MPa. This sample is above the critical threshold and we can conclude that $p_c < 62\%$. It is not possible to extrapolate A_c from the data. We know that E30 at 85 MPa is close to threshold, but we cannot accurately find the threshold itself. However, by modelling the void space geometry with the Stratified Continuum percolation construction (NOLTE and PYRAK-NOLTE, 1991) it is possible to make a quantitative estimate of p_c.

The percolation strength and spanning probabilities for Stratified percolation are shown in Figure 4 as functions of area fraction for sample sizes $L = 1, 1/2, 1/3, 1/6$. The probabilities were obtained by making 300 stratified percolation simulations for each area fraction. The relative sample sizes were identical to those used for the data in Figures 5 and 6. The simulations used three tiers with a scale factor of $b = 4.27$. The critical threshold in these simulations is $p_c = 0.5$. Above threshold the simulations agree quantitatively with the behavior of the data in Figures 5 and 6. The agreement between the data and simulations is independent of the experimental fracture specimen E30 or E32. This indicates that the area fraction is a general property that can be used to establish the percolation properties of a fracture. Accepting $p_c = 0.5$ as the percolation threshold for the data, the explicit dependence of the correlation length can be determined from the data. For sample E30 subjected to a stress of 85 MPa, the occupied area is $p = 0.62$, and the measured correlation length is approximately $\xi \approx 1$ mm. Substituting for ξ, p, and p_c in equation (3) allows us to find the proportionality constant between ξ and

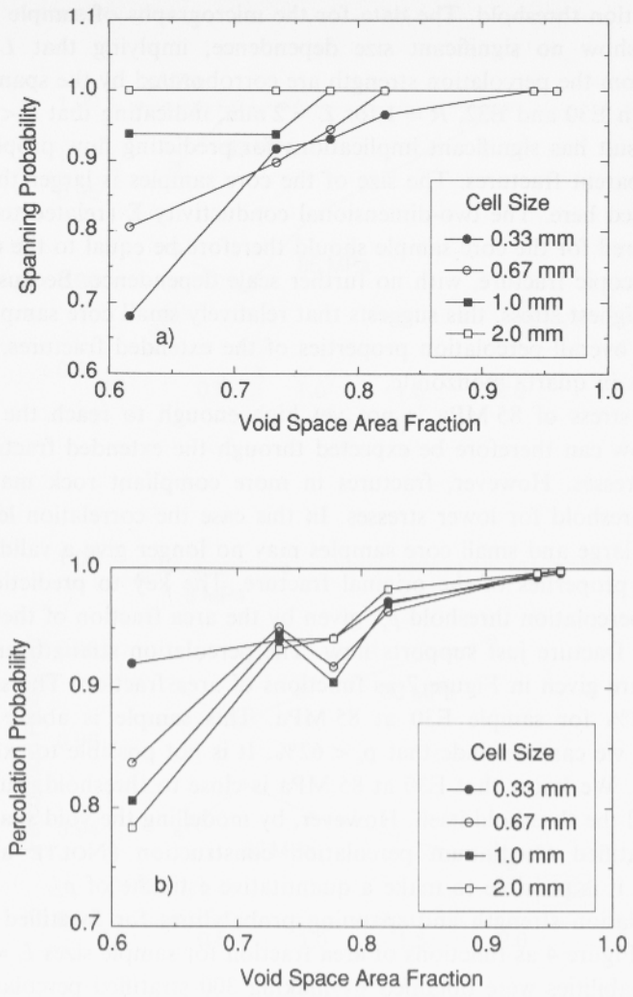

Figure 7
Spanning probability (a) and percolation probability (b) for all six micrographs as functions of the area fraction covered by the void spaces. Deviations for finite sizes occur only at the highest stress of 85 MPa for sample E30.

$(p - p_c)^{-\nu}$. This yields the explicit relationship

$$\xi = 6.4 \times 10^{-5}(p - 0.5)^{-1.3}\ \text{m} \tag{9}$$

for the correlation length for these fracture specimens. It is important to note that the correlation exponent $\nu = 4/3$ provides only a relatively weak dependence of the correlation length on the occupied area. Even for $p - p_c = 0.02$, which would occur only under extreme pressures, the correlation length would only be 1 cm. Therefore,

the hydraulic properties of the parent fractures are expected to be well represented by the properties measured on the small core samples.

4. *Multifractal Fracture Voids*

An important advance in the understanding of complex fractal structures was made with the recognition that some scaling patterns could be described as unions of multiple fractal sets, or multifractals. Multifractal patterns are quite common, arising naturally in patterns that have varying densities. For example, ore bodies are characterized by the grade of ore. If one considers the distribution of all ore bodies, independent of grade, the fractal dimension will be significantly different than the fractal dimension for only the highest grade ore (MANDELBROT, 1989). In this simple example, the fractal dimension is a function of the ore grade. There is no longer a single fractal dimension that describes the ore distribution, but a continuously varying fractal dimension that depends on how one weights the data. Significant discrepancies can arise when different techniques are used to measure the fractal dimension of a multifractal pattern or object. Different techniques may weight the pattern differently. These difficulties are eliminated by applying multifractal analysis. In this analysis, a multifractal is decomposed into its multiple moments. The set of all moments uniquely defines the object and ambiguity is removed.

Multifractals were developed to characterize turbulence and strange attractors of deterministic chaotic systems (FRISCH and PARISI 1983; PALADIN and VULPIANI, 1984; BENZI et al., 1984; GRASSBERGER and PROCACCIA, 1983, 1984]. Percolation systems were found to consist of multifractal sets (DE ARCANGELIS *et al.*, 1985, 1986; RAMMAL *et al.*, 1985, 1986; BHATTI and ESSAM, 1986; BLUMENFIELD *et al.*, 1986) when the bonds are assigned weights proportional to the voltage drops across the bonds. Other systems also show multifractality, such as aggregation processes (MEAKIN *et al.*, 1986; HALSEY *et al.*, 1986; AMITRANO *et al.*, 1986). In these processes, growth sites can be weighted according to their probability for growth. Sites at the tips have higher probability of growth than internal sites. The tips form a fractal subset with a lower fractal dimension than the fractal dimension for the full aggregate structure. In this section, we first described multifractal analysis, then present the multifractal analysis of the void space geometry in the fractured rock samples.

A. Multifractal Analysis

The box counting technique is one of the most widely used methods to obtain the fractal dimension D of a self-similar structure or pattern. One reason for the success of the box-counting technique is its ease of use. All that is required is to

count the number of boxes $N(L)$ of side L that are needed to cover the pattern. The fractal dimension is obtained through the expression

$$D = -d \ln N(L)/d \ln L. \tag{10}$$

The procedure can be implemented by successively subdividing the pattern in a regular grid with M cells of size L. A weight w_i can be defined for the ith cell such that $w_i = 1$ if the cell contains any part of the pattern, and $w_i = 0$ if the cell is completely empty. The number of boxes of size L covering the pattern is then

$$N(L) = \sum_{i=1}^{M} w_i. \tag{11}$$

The extension of this fractal analysis to include multifractals involves assigning a weight μ_i which is equal to the total "mass" enclosed in the ith cell (normalized to the total mass of the system). In the case of a black and white image, the mass would be the area covered by black. The mass μ_i is raised to a power q, where q expresses the mass moment of the distribution of masses that define the pattern. The definition for the weighted number of boxes $N(q, L)$ is

$$N(q, L) = \sum_{i=1}^{M} \mu_i^q \propto L^{-\tau(q)} \tag{12}$$

where the mass exponent $\tau(q)$ is given by

$$\tau(q) = -d \ln N(q, L)/d \ln L. \tag{13}$$

For the special case $q = 0$ (and only for this special case) the weighted number of boxes $N(q, L)$ reduces to the number of boxes needed to cover the pattern $N(L)$, yielding $\tau(q) = D$. For $q = 1$, then $\tau(q) = 0$ because $\sum_i \mu_i = 1$, for $i = 1, M$.

To find the connection between the mass exponent $\tau(q)$ and the fractal dimension that describes the qth mass moment of the pattern, it is necessary to look more closely at the definition of a multifractal (FEDER, 1988). A multifractal set S is the union of fractal subsets S_α, $S = \bigcup S_\alpha$, characterized by the parameter α. The subset S_α consists of points of mass distributed across the pattern. The mass μ_α in a cell of size L of the subset S_α varies as

$$\mu_\alpha \propto L^\alpha. \tag{14}$$

The parameter α is called the Lipschitz–Hölder exponent. The fractal dimension of the support of this mass distribution is given by $f(\alpha)$ defined through the expression

$$N(\alpha, L) = \rho(\alpha) L^{-f(\alpha)}\, d\alpha \tag{15}$$

in which $N(\alpha, L)$ is the number of boxes of side L that are needed to cover sets S_α in the range of α to $\alpha + d\alpha$. The density $\rho(\alpha)\, d\alpha$ is the number of sets from S_α to $S_{\alpha + d\alpha}$. It is important to note the distinction between α and $f(\alpha)$, even though both are scaling exponents. The fractal subset S_α consists of a distribution of mass. The

manner in which the *mass* is distributed in space defines α. The set of *points* in space that the support the subset S_α has the fractal dimension $f(\alpha)$. The fractal dimension $f(\alpha)$ is always less than the Euclidean dimension, $d = 2$ in our case. The exponent α, on the other hand, can have values larger than 2. Combining equations (12), (14), and (15) yields

$$\begin{aligned} N(q, L) &= \int d\alpha \mu_\alpha^q N(\alpha, L) \\ &\propto \int d\alpha \rho(\alpha) L^{-f(\alpha)} L^{\alpha q} \\ &\propto L^{-\tau(q)}. \end{aligned} \tag{16}$$

From the final expression one obtains the relationship

$$f(\alpha) = \tau(q) + \alpha q \tag{17}$$

giving the explicit dependence of $f(\alpha)$ on $\tau(q)$. The Lipshitz–Hölder exponent is a function of q, and the relation between $\alpha(q)$ and q is given by finding the maximum value of equation (16). This is done by maximizing the exponent $\alpha q - f(\alpha)$ in equation (16) for a given q. Thus,

$$\frac{d}{d\alpha} \{\alpha q - f(\alpha)\}_{q = \text{const.}} = q - \frac{\partial f}{\partial \alpha} = 0. \tag{18}$$

and

$$\alpha(q) = -\frac{\partial}{\partial q} \tau(q). \tag{19}$$

Equations (17) and (19) make it possible to describe the fractal dimension $f(\alpha(q))$ for varying q which we will write as $f(q)$, or for varying α which we will write as $f(\alpha)$, based on the weighted number of boxes given by equation (12). The limiting behavior of $f(\alpha)$ is given in Table 1 (STAUFFER, 1985).

Table 1

Limiting behavior for $f(\alpha)$

q	$\tau(q)$	$\alpha = -d\tau(q)/dq$	$f = \alpha q + \tau(q)$
$q \to -\infty$	$-q\alpha_{\max}$	$\alpha_{\max}$	0
$q = 0$	D	α_0	$f_{\max} = D$
$q \to +\infty$	$-q\alpha_{\min}$	$\alpha_{\min}$	0

where $\alpha_{\max}$ corresponds to the subset of smallest masses and $\alpha_{\min}$ corresponds to the subset of largest masses.

The multifractal analysis described in the preceding paragraphs was applied to the experimental micrographs of Figures 2 and 3 by considering the black areas (the void spaces) as the multifractal set S. The weighted number of boxes $N(q, L)$ from equation (12) was calculated for cell sizes L ranging from 0.2 mm to 2 mm. The dependence of $N(q, L)$ on L is shown in Figure 8 using sample E30 as an example. The different lines are for different values of the exponent q in equation (12). The mass exponent $\tau(q)$ is given by the slopes of the lines on the log-log plot in Figure 8, and is shown in Figure 9. The pattern scales, producing power law dependences over one order of magnitude for sizes between 0.2 mm and 2 mm. The fractal dimension, $f(q)$, is obtained through equations (17) and (19).

The fractal dimensions $f(q)$ as functions of the mass moment q are shown in Figure 10. When q is negative, cells with small amounts of mass (void space) are weighted preferentially over dense regions. In this range of values of q, the fractal subset consists of the edges of the voids or isolated small voids. The fractal dimensions of these subsets decrease to zero as $q \to -\infty$. For positive q, cells with large amounts of mass (void space area) are weighted preferentially. The fractal subsets for positive values of q therefore consist of the large void spaces with little or no contact areas. Increasing q in the positive direction reduces the fractal dimension because only the boxes that are fully occupied by void space are important, and the set of these boxes have smaller fractal dimensions. For $q = 0$,

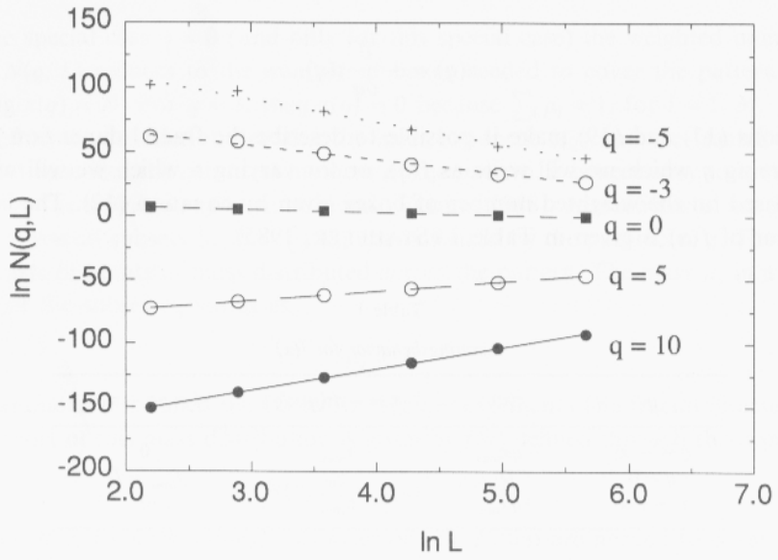

Figure 8
The weighted box numbers $N(q, L)$ of equation (12) as functions of L for selected values of the exponent q. These data are from sample E30 at 85 MPa for a region covering 4 square millimeters.

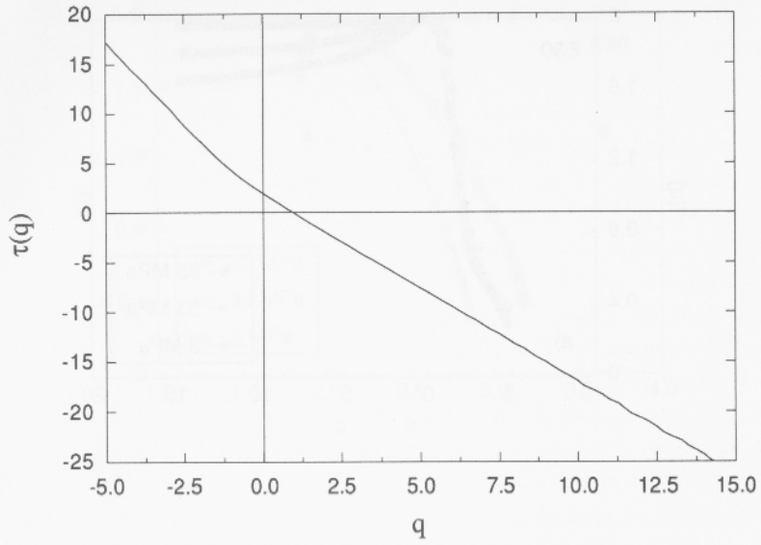

Figure 9
The mass exponent $\tau(q)$ derived from the slopes of the data in Figure 8.

$f(q)$ is equal to the fractal dimension of the 2-dimensional pattern. During the box counting any box that has any amount of metal (void space) is therefore weighted equally. The fractal dimensions for the micrographs are all close to $D \approx 2$. In the micrographs, even relatively large areas of contact (white) can have small voids. Therefore, nearly all boxes at all sizes contain void space, producing a fractal dimension close to the Euclidean dimension $E = 2$. The fractal dimensions obtained here are significantly higher than the fractal dimensions described in NOLTE *et al.* (1989) for the same samples. This difference reflects a different weighting during the box counting. In NOLTE *et al.* (1989), only the largest clusters of void spaces in a box contributed to the mass enclosed in that box. This criterion for box counting discounts the small, disconnected clusters. Therefore the fractal dimensions measured there correspond to the fractal dimension of the spanning cluster.

The mass moment q does not give a complete description of the structure of the multifractal. The Lipschitz–Hölder exponent α is more closely related to the scaling properties of the multifractal pattern and can provide a unique description of the mass distributions in the patterns. The fractal dimensions $f(\alpha)$ of the micrographs of Figures 2 and 3 are shown in Figure 11 as functions of the parameter α. A serious question can be raised about the validity of performing a multifractal analysis on a black and white pattern, as for the micrographs of the metal casts. In a multifractal, each point in space is assigned a density. Multifractal analysis

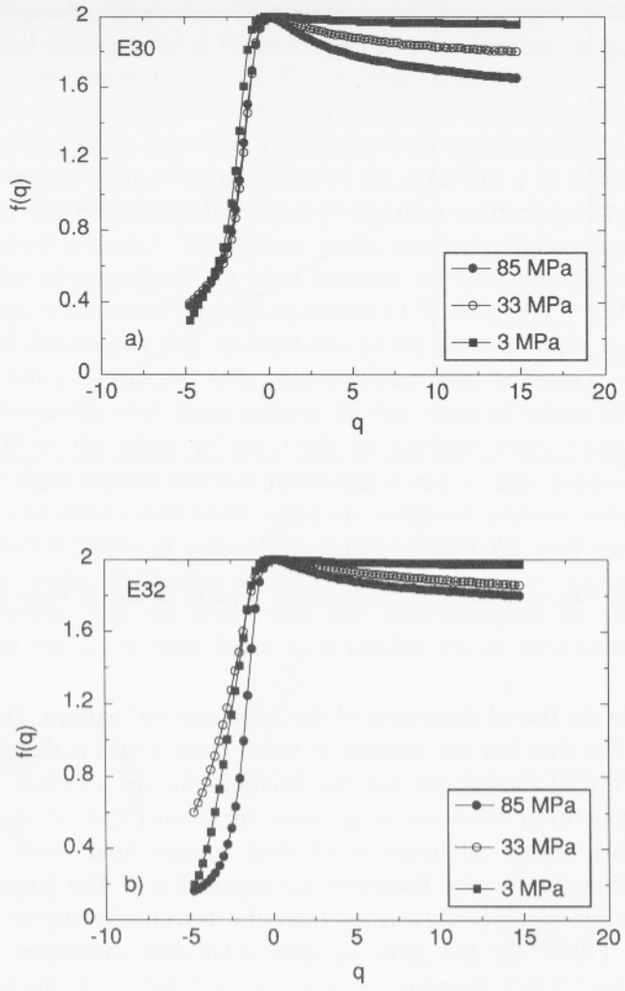

Figure 10
Fractal dimension as a function of the mass moment q for (a) specimen E30 and (b) specimen E32. The results for the three stresses are shown.

reduces the complicated density distribution into subsets of a given density. Each subset has a specific fractal dimension. In a black and white pattern, however, density information is lost and values of 1 or 0 are assigned to each point in space. Even in this case, the multifractal analysis can yield meaningful information, allowing an interpretation of the $f(\alpha)$ curve. The metal cast of the fracture is composed of finite clusters. The clusters vary in area from square microns to square millimeters. Each value of α in the $f(\alpha)$ curve correspond to a subset of clusters of a given area. The set of smallest clusters (corresponding to $\alpha \approx 3$), have a small

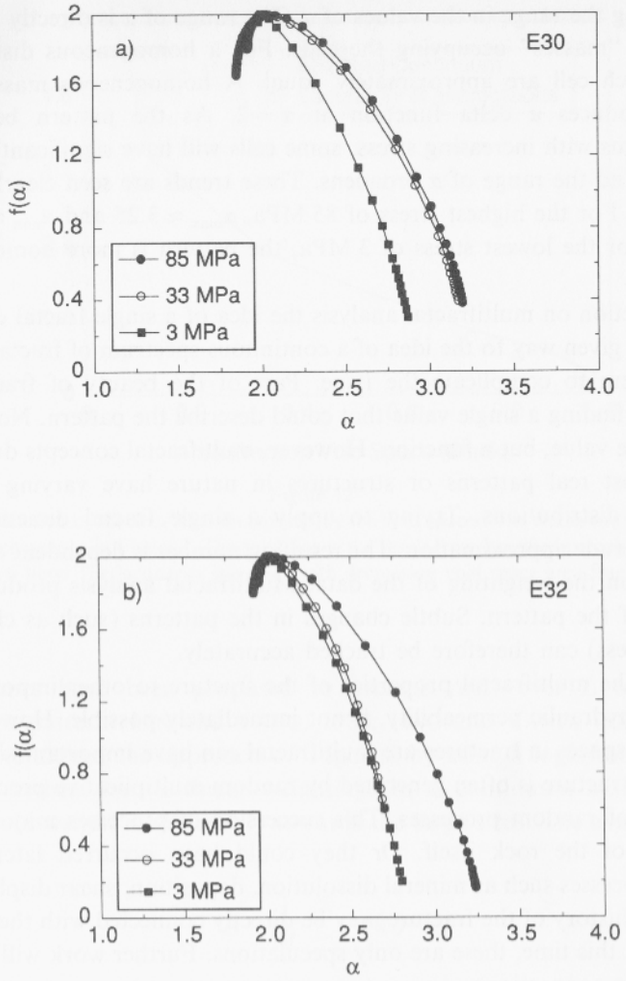

Figure 11
Fractal dimension as a function of the exponent α for (a) specimen E30 and (b) specimen E32. The range of α increases for increasing stress on the samples as the contact area becomes more inhomogeneous.

fractal dimension because they are widely scattered and scale weakly with box size. In the other extreme, the largest cluster (corresponding to $\alpha \approx 2$) homogeneously covers the micrograph efficiently, given $D \approx 2$. For $\alpha < 2$, the fractal dimension drops precipitously because no cluster is larger than the spanning cluster. Based on this discussion, we find that multifractal analysis can still be interpreted usefully to apply to complex patterns that do not have a continuously varying density.

There is a clear trend in the $f(\alpha)$ curves as stress is increased on the samples. The width of the parameter α increases with increasing stress. This effect can be understood

by considering the range in the values of α. The range of α is directly related to the range in the "masses" occupying the cells. For a homogeneous distribution, the masses in each cell are approximately equal. A homogeneous mass distribution therefore produces a delta function at $\alpha = 2$. As the pattern becomes more inhomogeneous with increasing stress, some cells will have significantly more mass than others and the range of α broadens. These trends are seen clearly in the data in Figure 11. For the highest stress of 85 MPa, $\alpha_{max} \approx 3.25$ and $\alpha_{min} \approx 1.80$, giving $\Delta\alpha = 1.45$. For the lowest stress of 3 MPa, the pattern is more homogeneous and $\Delta\alpha = 0.9$.

In this section on multifractal analysis the idea of a single fractal dimension for a pattern has given way to the idea of a continuous spectrum of fractal dimensions. This may seem to complicate the issue. Part of the beauty of fractals was the possibility of finding a single value that could describe the pattern. Now there is no longer a single value, but a function. However, multifractal concepts do simplify the problem. Most real patterns or structures in nature have varying densities, or altitudes, or distributions. Trying to apply a single fractal dimension to such patterns is a crude approximation. The resulting number is dependent on the chosen cutoffs, and on the weighting of the data. Multifractal analysis produces a unique description of the pattern. Subtle changes in the patterns (such as changes under increasing stress) can therefore be tracked accurately.

Relating the multifractal properties of the fracture to other important properties, such as hydraulic permeability, is not immediately possible. However, the fact that the void spaces in fractures are multifractal can have important significance. A multifractal structure is often generated by random multiplicative processes, i.e., by a succession of random processes. This succession of processes may occur during the fracture of the rock itself. Or they could have occurred later, caused by successive processes such as mineral dissolution, deposition, shear displacement, etc. The geologic history of the fracture may be directly connected with the shape of the $f(\alpha)$ curve. At this time, these are only speculations. Further work will be necessary to uncover the connections.

B. Lacunarity

A closely related property to the fractal dimension is lacunarity. The term "lacunarity" was coined by MANDELBROT (1983) to refer to the magnitude of the "gaps" in the pattern. It also refers to the prefactor in the number-size relationship. One common definition of lacunarity $\Lambda(L)$ is the mean-square deviation of the occupied area fractions for a certain size L

$$\Lambda(L) = \frac{\langle A^2(L)\rangle - \langle A(L)\rangle^2}{\langle A(L)\rangle^2} \tag{20}$$

where $A(L)$ is the fraction of the area that is occupied in a square of linear size L.

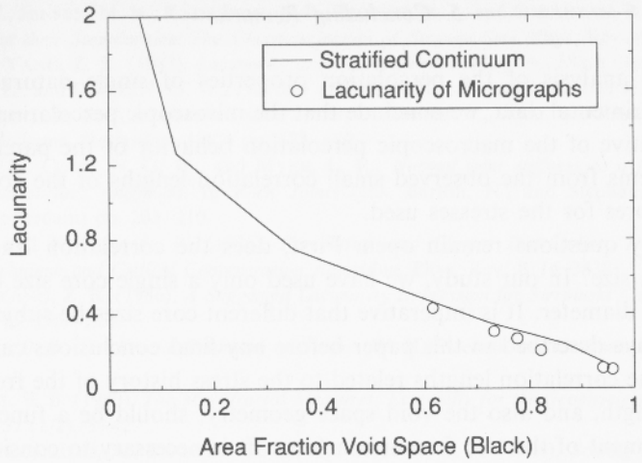

Figure 12
Lacunarity as a function of the area fraction covered by the void spaces. The circles are the experimental data from the micrographs in Figure 2. The solid line is the result from stratified percolation simulations for two tiers. The lacunarity increases with decreasing void space area fractions.

Various schemes have been proposed to average $\Lambda(L)$ over L to obtain the lacunarity of a pattern (LIN and YANG, 1986; HAO and YANG, 1987; TAGUCHI, 1987). We have altered the approach of Taguchi, by using a logarithmic weighting of the $\Lambda(L)$, rather than a linear weighting. In a continuum system, a linear weighting would weight more heavily towards the large sizes. The average lacunarity Λ is

$$\Lambda = \frac{1}{M}\sum_{i=1}^{M} \Lambda(2^i) \tag{21}$$

for M cells. The factor of 2 is the scale factor between observation scales L_i, where $L_i = 2^i$. This factor of 2 is arbitrary, and is chosen for simplicity.

The experimental lacunarity from the micrographs in Figures 2 and 3 is shown in Figure 12 as a function of area fraction covered by void space. The data are compared to simulations of stratified percolation using two tiers. The lacunarity increases as the "gaps," or contact areas, increase. The lacunarity diverges as $A \to 0$ as the denominator of equation (20) vanishes. Lacunarity plays a secondary role in the description of scaling patterns, but can have effects on such real properties as fracture specific stiffness. It has been shown (HOPKINS and COOK, 1987, 1990), that for the same contact area, fractures with different distributions of the contact area have different fracture stiffnesses. The lacunarity of a fracture gives a measure of this distribution and should therefore influence the mechanical stiffness of the fracture under stress.

5. Concluding Remarks

From this analysis of the percolation properties of single natural fractures, based on experimental data, we conclude that the miroscopic percolation properties are representative of the macroscopic percolation behavior of the parent fracture. This result stems from the observed small correlation lengths of the contact areas in these fractures for the stresses used.

Several key questions remain open. First, does the correlation length change with specimen size? In our study, we have used only a single core size of fifty-two centimeters in diameter. It is imperative that different core sizes be subjected to the analysis we have described in this paper before any final conclusions can be made. Second, are the correlation lengths related to the stress history of the fracture? The correlation length, and also the void space geometry, should be a function of the shear displacement of the two fracture surfaces. It is necessary to consider erosion and precipitation that occur when fluids are present over the lifetime of the fracture. These processes may relate directly to the finite-size and multiscaling properties of fractures, and ultimately to determining the hydraulic properties of natural fractures.

References

ARMITRANO, C., CONIGLIO, A., and DI LIBERTO, F. (1986), *Growth Probability Distribution in Kinetic Aggregation Processes*, Phys. Rev. Lett. *57*, 1016.

BENZI, R., PALADIN, G., PARISI, G., and VULPIANI, A. (1984), *On the Multifractal Nature of Fully Developed Turbulence and Chaotic Systems*, J. Phys. A *17*, 3521–3531.

BHATTI, F. M., and ESSAM, J. W. (1986), *Series Expansion Study of the Distribution of Currents in the Elements of a Random Diode-insulator Network*, J. Phys. A *19*, L519–L525.

BLUMENFIELD, R., MEIR, Y., HARRIS, A. B., and AHARONY, A. (1986), *Infinite Set of Exponents Describing Physics on Fractal Networks*, J. Phys. A *19*, L791.

BROWN, S. R., and SCHOLZ, C. H. (1985), *Closure of Random Elastic Surfaces in Contact*, J. Geophys. Res. *90*, 5531–5545.

BROWN, S. R., KRANZ, R. L., and BONNER, B. P. (1986), *Correlation between the Surfaces of Natural Rock Joints*, Geophys. Res. Lett. *13*, 1430–1434.

DE ARCANGELIS, L., REDNER, S., and CONIGLIO, A. (1985), *Anomalous Voltage Distribution of Random Resistor Networks and a New Model for the Backbone at the Percolation Threshold*, Phys. Rev. B *31*, 4725.

DE ARCANGELIS, L., REDNER, S., and CONIGLIO, A. (1986), *Multiscaling Approach in Random Resistor and Random Superconducting Networks*, Phys. Rev. B *34*, 4656.

DULLIEN, F. A. L. (1981), *Wood's Metal Porosimetry and its Relation to Mercury Porosimetry*, Powder Technology *29*, 109–116.

FEDER, J., *Fractals* (Plenum Press, New York 1988).

FRISCH, U., and PARISI, G. (1983), *Turbulence and Predictability of Geophysical Flows and Climate Dynamics*, Varenna Summer School LXXXVIII.

GRASSBERGER, P., and PROCACCIA, I. (1983), *Characterization of Strange Attractors*, Phys. Rev. Lett. *50*, 346–349.

GRASSBERGER, P., and PROCACCIA, I. (1984), *Dimensions and Entropies of Strange Attractors from a Fluctuating Dynamics Approach*, Physica D *13*, 34–54.

HALSEY, T. C., JENSEN, M. H., KADANOFF, L. P., PROCACCIA, I., and SHRAIMAN, B. I. (1986), *Fractal Measures and their Singularities: The Characterization of Strange Sets*, Phys. Rev. A *33*, 1141.

HAO, L., and YANG, Z. R. (1987), *Lacunarity and Universality*, J. Phys. A., Math Gen. *20*, 1627–1631.

HOPKINS, D. L., and COOK, N. G. W., *Fracture stiffness and aperture as a function of applied stress and contact geometry*. In *Rock Mechanics* (eds. Farmer, I., Daemen, J., Desai, C., Glass, C., and Neuman S.) (A. A. Balkema, Rotterdam 1987) pp. 673–680.

HOPKINS, D. L., COOK, N. G. W., and MYER, L. R., *Normal joint stiffness as a function of spatial geometry and surface roughness*. In *Rock Joints* (eds. Barton, N., and Stephansson, O.) (A. A. Balkema, Rotterdam) pp. 203–210.

HOSHEN, J., and KOPELMAN, R. (1976), *Percolation and Cluster Distribution. I. Cluster Multiple Labeling Technique and Critical Concentration Algorithm*, Phys. Rev. B *14*, 3438.

LIN, B., and YANG, Z. R. (1986), *A Suggested Lacunarity Expression for Sierpinski Carpets*, J. Phys. A., Math Gen. *19*, L49–L52.

MANDELBROT, B. B., *The Fractal Geometry of Nature* (W. H. Freeman and Company, New York 1983) 468 pp.

MANDELBROT, B. B. (1989), *The Multifractal Measures, Especially for the Geophysicist*, Pure and Appl. Geophys. *131* (1/2), 5–42.

MEAKIN, P., CONIGLIO, A., STANLEY, H. E., and WITTEN, T. A. (1986), *Scaling Properties for the Surfaces of Fractal and Nonfractal Objects: An Infinite Hierarchy of Critical Exponents*, Phys. Rev. A *34*, 3325.

NEUZIL, C. E., and TRACEY, J. V. (1981), *Flow Through Fractures*, Water Resources Res. *17* (1), 191–199.

NOLTE, D. D. (1989), *Invariant Fixed Point in Stratified Continuum Percolation*, Phys. Rev. A *40* (8), 4817–4819.

NOLTE, D. D., PYRAK-NOLTE, L. J., and COOK, N. G. W. (1989), *The Fractal Geometry of Flow Paths in Natural Fractures in Rock and the Approach to Percolation*, Pure and Appl. Geophys. *131* (1/2), 271.

NOLTE, D. D., and PYRAK-NOLTE, L. J. (1991), *Stratified Continuum Percolation: Scaling Geometry of Hierarchical Cascades*, Phys. Rev. A *44*, 6320–6333.

PALADIN, G., and VULPIANI, A. (1984), *Characterization of Strange Attractors as Inhomogeneous Fractals*, Lett. Nuovo Cimento *41*, 82–89.

PFEUTY, P., and TOULOUSE, G., *Introduction to the Renormalization Group and to Critical Phenomena* (John Wiley and Sons, London 1975).

PYRAK-NOLTE, L. J., MEYER, L. R., COOK, N. G. W., and WITHERSPOON, P. A., *Hydraulic and mechanical properties of natural fractures in low permeability rock*. In *Proceedings, International Society for Rock Mechanics, 6th International Congress on Rock Mechanics, Montreal, Canada, August 1987* (A. A. Balkema, Rotterdam 1987) pp. 225–231.

PYRAK-NOLTE, L. J. (1991), *The Feasibility of Using Wood's Metal Porosimetry to Measure the Fracture Void Geometry of Cleats in Coal*, Topical Report, Gas Research Institute GRI-91-0373, 22 pp.

RAMMAL, R., TANNOUS, C., BRETON, P., and TREMBLAY, A. M. S. (1985), *Flicker (1/f) Noise in Percolation Networks: A New Hierarchy of Exponents*, Phys. Rev. Lett. *54*, 1718.

RAMMAL, R., TANNOUS, C., and TREMBLAY, A. M. S. (1986), *1/f Noise in Random Resistor Networks: Fractals and Percolating Systems*, Phys. Rev. A *31*, 2662.

RAVEN, K. G., and GALE, J. E. (1985), *Water Flow in a Natural Rock Fracture as a Function of Stress and Sample Size*, Internat. J. Rock Mechanics and Mining Sc. and Geomech. Abstracts *22* (4), 251–261.

REDNER, S. (1990), *Random Multiplicative Processes: An Elementary Tutorial*, Am. J. Phys. *58*, 267–273.

STANLEY, H. E., *Introduction to Phase Transitions and Critical Phenomena* (Oxford University Press, New York 1971).

STAUFFER, D., *Introduction to Percolation Theory* (Taylor and Francis, London 1985).

SWAN, G. (1983), *Determination of Stiffness and Other Joint Properties from Roughness Measurements*, Rock Mechanics and Engineering *6*, 19–38.

SWANSON, B. F. (1979), *Visualizing Pores and Non-wetting Phase in Porous Rock*, J. Petroleum Technology *31*, 10–18.

TAGUCHI, Y. (1987), *Lacunarity and Universality*, J. Phys. A., Math Gen. *20*, 6611–6616.

TSANG, Y. W., and WITHERSPOON, P. A., (1983), *The Dependence of Fracture Mechanical and Fluid Flow Properties on Surface Roughness and Sample Size*, J. Geophys. Res. *88* (B3), 2359–2366.

WILSON, K. G., and KOGUT, J. (1974), *The Renormalization Group and the Epsilon Expansion*, Physics Reports *12C*, 75–200.

WILSON, K. G. (1975), *The Renormalization Group: Critical Phenomena and the Kondo Problem*, Adv. Phys. *47* (4), 773–840.

WILSON, K. G. (1979), *Problems in Physics with Many Scales of Length*, Scientific America *241* (2), 158–179.

WITHERSPOON, P. A., AMICK, C. H., GALE, J. E., and IWAI, K. (1979), *Observations of a Potential Size Effect in Experimental Determination of the Hydraulic Properties of Fractures*, Water Resources Res. *15* (5), 1142.

YADAV, G. D., DULLIEN, F. A. L., CHATZIS, I., and MACDONALD, I. F. (1984), *Microscopic Distribution of Wetting and Non-wetting Phases in Sandstones during Immiscible Displacements*, SPE 13212, Society of Petroleum Engineers of AIME, Dallas, Texas.

ZHENG, Z. (1989), *Compressive Stress-induced Microcracks in Rocks and Applications to Seismic Anisotropy and Borehole Stability*, Ph.D. Thesis, University of California, Berkeley.

(Accepted April 2, 1992)